International Journal of Modern Physics C
Vol. 29, No. 9 (2018) 1850117 (15 pages)

DOI: 10.1142/S0129183118501176

Rarefied transitional flow through diverging nano and microchannels: A TRT lattice Boltzmann study

Soroush Fallah Kharmiani and Ehsan Roohi*

Department of Mechanical Engineering
Ferdowsi University of Mashhad
Mashhad 91779-1111, Iran
**e.roohi@ferdowsi.um.ac.ir*

Received 4 September 2018
Accepted 30 October 2018
Published

Rarefied isothermal gaseous flow through long diverging micro and nanochannels is investigated in this paper using the two-relaxation-time (TRT) lattice Boltzmann method (LBM). The simulations are performed over a wide range of Knudsen number, pressure ratio, and divergence angle. The Bounce-Back Specular Reflection (BSR) slip boundary condition is applied and is connected to the second-order slip boundary condition coefficients by means of the antisymmetric relaxation time and the bounce-back portion parameter. The effects of the slip coefficients on the wall and centerline Mach numbers, as well as the mass flow rates, are investigated. The numerical results are validated with those of the direct simulation Monte Carlo (DSMC) reported in the literature. The results show that the local pressure distributions are almost independent of the slip coefficients with excellent agreements with DSMC over a wide range of the divergence angle. Our results demonstrate that there is a specific divergence angle at each pressure ratio where the local unbounded Knudsen and, as a result, Mach numbers remain constant along the channel. This observation is almost independent of the slip coefficients, and the underlying reason is that the pressure drop is compensated by an increase in the channel area.

Keywords: Divergent microchannel; TRT LBM; rarefied flow; BSR slip boundary condition; model validation.

1. Introduction

The rarefied gaseous flow through nanochannels with sudden or gradual expansion has widespread engineering applications, such as hard disk drives. While considerable work is carried out on investigating the rarefied gas flow through micro and nanochannels with uniform cross-sections, e.g. Refs. 1–7, much fewer researches are reported on microchannels with nonuniform cross-sections. Based on the kinetic equation, Sharipov and Bertoldo[8] proposed a method for determining the mass flow rate through a long tube with a variable radius. Stevanovic[9] analytically investigated

*Corresponding author.

the 2D microgaseous flow through slowly varying microchannel using the perturbation method. Hemadri *et al.*[10] experimentally investigated the rarefied gaseous flow through diverging microchannel and existence of the Knudsen minimum was reported. Akbari *et al.*[11] proposed a model for predicting the pressure loss in non-uniform microchannels with arbitrary cross sections in the slip regime. Ebrahimi and Roohi[12] simulated the 2D rarefied gas flow through a diverging microchannel using the DSMC method. Kiselev *et al.*[13] studied the supersonic gas flows in radial micronozzles. Darbandi and Roohi[14] investigated the rarefied gaseous flow through backward-facing steps and reported that the separation length is highly reduced as the rarefaction is increased approaching the transition regime. Mahdavi *et al.*[15] and Mahdavi and Roohi[16] further studied rarefied flow through step geometries using the DSMC method. Recently, Gavasane *et al.*[17] also numerically investigated the rarefied gas flows in backward facing microstep using the DSMC method.

As an alternative numerical method, the lattice Boltzmann method (LBM)[18–22] takes advantage of relative simplicity, computational efficiency, and simulating flows involving complex geometries such as the porous media. Furthermore, the kinetic-based nature of the LBM makes it a robust tool for simulating complex physics such as multi-phase,[23–25] and micro/nano gaseous flows[26,27] including the shale gas flow. The method is successfully applied to the simulation of the rarefied gas flows between two flat walls up to the end of the transition regime. Wang *et al.*[28] reviewed the application of the LBM for simulating the isothermal microgaseous flows. The method is also applied to the gas flow in a microchannel with sudden expansion/contraction. Agrawal *et al.*[29] investigated the rarefied gas flow in a microchannel with sudden expansion or contraction in the slip regime using the LBM. Liou and Lin[30] also applied the LBM for simulating the microchannel gas flow with sudden expansion/contraction for a wide range of the Knudsen number. Recently, Li *et al.*[31] investigated the rarefied gas flow through channels with sudden and gradual contraction junction with application in the shale gas flow using the multiple-relaxation-time (MRT) LBM.

In order to simulate rarefied flows involving the off-lattice curved/inclined boundaries in LBM, Guo *et al.*[32] approximated the curved boundary with the stair-step mesh. The approximated wall was taken to be located at half-way of each cut link, i.e. $\Delta = 0.5$. Furthermore, they implemented the Diffuse-Bounce-Back (DBB) slip boundary condition and could simulate the rarefied cylindrical Couette flow and capture the velocity inversion phenomenon using the MRT collision operator. Later, Tao *et al.*[33] extended the DBB slip boundary condition for arbitrary values of Δ using the MRT LBM. Recently, the sputtering boundary condition[34,35] is developed and utilized for determining amounts of reactants and products in a chemical reaction occurring at solid boundaries of a catalyst.

In this paper, the TRT LBM proposed by Ginzburg[36] is utilized. It was reported in the literature that values of the other relaxation times in the MRT LBM almost have no influence on simulation results of the rarefied gas flows.[33] Therefore, it can be concluded that the TRT LBM is robust enough for modeling such flows. Clearly, the

TRT LBM takes advantage of a lower computational cost, rapid simulation time and an easier coding. The TRT LBM was successfully applied by Norouzi *et al.*[37] for simulating rarefied Poiseuille flow between two parallel plates in the entire range of the transition regime.

An inspection of the published literature reveals that application of the LBM for simulating the rarefied gas flow through long diverging microchannels is not reported. Here, the TRT LBM is employed to simulate divergent micro and nanochannels for the first time. The divergent wall is approximated with the stair-step mesh, and the Bounce-Back Specular Reflection (BSR) slip boundary condition is applied. The power-law (PL) wall function is implemented to capture the Knudsen layer effects in the transition regime. Pressure and Knudsen number distributions, slip, and centerline Mach numbers, and mass flow rate are studied and compared with DSMC results, where available, at different divergence angles. Furthermore, it is shown that there is a threshold divergence angle at a given pressure ratio where the unbounded Knudsen number and Mach number remain constant along the channel.

2. Numerical Model

The governing equation of the TRT LBM is expressed as

$$f_i(\boldsymbol{x} + \boldsymbol{e}_i\delta t, t + \delta t) - f_i(\boldsymbol{x}, t) = -\frac{1}{\tau_s}(f_i^s(\boldsymbol{x}, t) - f_i^{\mathrm{seq}}(\boldsymbol{x}, t)) - \frac{1}{\tau_a}(f_i^a(\boldsymbol{x}, t) - f_i^{\mathrm{aeq}}(\boldsymbol{x}, t)), \quad (1)$$

where $\boldsymbol{x}$ is the spatial position, $\boldsymbol{e}_i$ the discrete velocity in the ith direction, δt the time step, f_i the particle distribution function, and sub/super-scripts s and a stand for symmetric and antisymmetric parts, respectively. Compared with the MRT relaxation times, $\tau_s = \tau_\nu$ and $\tau_a = \tau_q$, where τ_ν and τ_q are the relaxation times related to the shear stress and heat flux, respectively.

The equilibrium distribution function (EDF) is given by

$$f_i^{\mathrm{eq}} = \omega_i\rho\left[1 + \frac{\boldsymbol{e}_i \cdot \boldsymbol{V}}{c_s^2} + \frac{(\boldsymbol{e}_i \cdot \boldsymbol{V})^2}{2c_s^4} - \frac{\boldsymbol{V} \cdot \boldsymbol{V}}{2c_s^2}\right], \quad (2)$$

where $c_S = c/\sqrt{3}$ is the speed of sound, and $c = \delta x/\delta t$ is the lattice speed with δx as the lattice spacing.

The symmetric and antisymmetric distribution functions are calculated as follows:

$$f_i^s = \frac{1}{2}(f_i + f_{-i}), \quad f_i^a = \frac{1}{2}(f_i - f_{-i}), \quad (3)$$

$$f_i^{\mathrm{seq}} = \frac{1}{2}(f_i^{\mathrm{eq}} + f_{-i}^{\mathrm{eq}}), \quad f_i^{\mathrm{aeq}} = \frac{1}{2}(f_i^{\mathrm{eq}} - f_{-i}^{\mathrm{eq}}), \quad (4)$$

where $-i$ is the opposite direction of i.

For the D2Q9 lattice model used in this paper, the discrete velocities and the weight factors are given by

$$\boldsymbol{e}_i = c\begin{bmatrix} 0 & 1 & 0 & -1 & 0 & 1 & -1 & -1 & 1 \\ 0 & 0 & 1 & 0 & -1 & 1 & 1 & -1 & -1 \end{bmatrix}, \tag{5}$$

$$\omega_i = \begin{cases} 4/9, & i = 0, \\ 1/9, & i = 1,2,3,4, \\ 1/36, & i = 5,6,7,8. \end{cases} \tag{6}$$

The fluid macroscopic density, velocity and pressure are given by

$$\rho = \sum_i f_i, \quad \rho \boldsymbol{V} = \sum_i f_i \boldsymbol{e}_i, \quad P = \rho c_s^2. \tag{7}$$

The symmetric relaxation time is related to the Knudsen number as follows[38]:

$$\tau_s = \sqrt{\frac{6}{\pi}}\frac{Kn_e H}{\delta x} + 0.5, \tag{8}$$

where Kn_e is the effective Knudsen number and H local height of the channel in case of the divergence channel. Effects of the Knudsen layer in the transition regime is considered by implementing the PL wall function proposed by Dongari *et al.*,[39] which is reported to be applicable over a wide range of Knudsen number in the transition regime:

$$Kn_e = Kn\beta_{PL}, \tag{9}$$

$$\begin{aligned} \beta_{PL} = 1 - \frac{1}{96}\Bigg[&\left(1 + \frac{\frac{H}{2} - y}{\lambda}\right)^{-2} + \left(1 + \frac{\frac{H}{2} + y}{\lambda}\right)^{-2} \\ &+ 4\sum_{k=1}^{8}\left(1 + \frac{\frac{H}{2} - y}{\lambda\cos\frac{(2k-1)\pi}{32}}\right)^{-2}\Bigg] + 4\sum_{k=1}^{8}\left(1 + \frac{\frac{H}{2} + y}{\lambda\cos\frac{(2k-1)\pi}{32}}\right)^{-2} \\ &+ 2\sum_{k=1}^{7}\left(1 + \frac{\frac{H}{2} - y}{\lambda\cos\frac{k\pi}{16}}\right)^{-2} + 2\sum_{k=1}^{7}\left(1 + \frac{\frac{H}{2} + y}{\lambda\cos\frac{k\pi}{16}}\right)^{-2}, \end{aligned} \tag{10}$$

where Kn is the unbounded Knudsen number. Effects of the channel walls (Kn layer) are not considered in the unbounded Knudsen number. Therefore, the Knudsen number needs to be corrected and the Kn layer effects included in the transitional regime, which is accomplished by implementing the PL wall function. The effective Knudsen number (Kn_e) is then calculated by modifying the unbounded Knudsen number given by Eq. (9). Indeed, the Kn_e governs the flow in the micro/nano-channel. As mentioned, H is the height of the channel which is no longer constant in case of the divergent channel, and y is the vertical coordinate of nodes measured from the channel symmetry axis. The mean free path equals $\lambda = Kn(x) \cdot H(x)$. For the isothermal flow in the divergent channels, the following relation can be deduced for

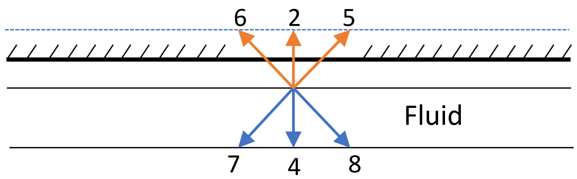

Fig. 1. (Color online) A flat solid boundary with known (orange) and unknown (blue) distribution functions.

the local unbounded Knudsen number:

$$\lambda_i P_i = \lambda P \rightarrow Kn_i H_i P_i = Kn.H.P \rightarrow Kn(x) = \frac{Kn_i P_i}{P(x)} \frac{H_i}{H(x)}. \tag{11}$$

In this paper, the BSR slip boundary condition is employed. For example, for the flat wall shown in Fig. 1, the half-way BSR is applied as follows:

$$\begin{aligned} f_4 &= f'_2, \\ f_7 &= r f'_5 + (1-r) f'_6, \\ f_8 &= r f'_6 + (1-r) f'_5, \end{aligned} \tag{12}$$

where f' denotes the post-collision distribution function and r determines the bounce-back portion. Clearly, setting $r = 1$ reduces the boundary condition to the half-way bounce-back and $r = 0$ to the specular wall.

As schematically depicted in Fig. 2, the divergent wall is approximated with the half-way stair-step Cartesian mesh such that the approximated wall is located at the middle of each cut-link between the immediate fluid and solid nodes adjacent to the actual wall. Apparently, the approximated wall would better represent the actual one with a finer mesh resolution.

As observed in Fig. 2, the approximated wall consists of a collection of flat walls; thus the BSR can still be applied easily with special cares of the nodes adjacent to the steps. The slip velocity as a result of applying the BSR boundary condition on a flat

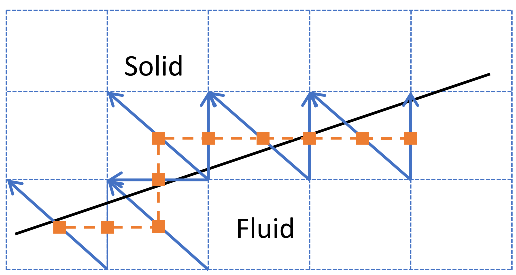

Fig. 2. (Color online) Schematic picture representing the actual wall (solid) and the approximated wall (dashed).

wall is given by[38]:

$$U_s = \frac{4(1-r)}{r}\sqrt{\frac{6}{\pi}}Kn + \frac{2\varpi}{\pi(\tau_s - 0.5)^2}Kn^2, \tag{13}$$

where $\varpi = 16(\tau_s - 0.5)(\tau_a - 0.5) - 3$. On the other hand, the analytical slip velocity arising from applying the second-order slip boundary condition $u_s = L_1\lambda\frac{\partial u}{\partial y}|_{\text{wall}} - L_2\lambda^2\frac{\partial^2 u}{\partial y^2}|_{\text{wall}}$ is obtained to be

$$U_s = 4L_1 Kn + 8L_2 Kn^2. \tag{14}$$

Therefore, equating Eqs. (13) and (14) leads to the following relations:

$$r = \left(1 + \sqrt{\frac{\pi}{6}}L_1\right)^{-1}, \tag{15}$$

$$\tau_a = \tau_q = 0.5 + \frac{4\pi L_2(\tau_s - 0.5)^2 + 3}{16(\tau_s - 0.5)}. \tag{16}$$

Although these relations are extracted for the Poiseuille flow between two parallel plates, they can also be used for cases with curved or inclined surfaces.[33,40]

3. Results and Discussion

A schematic drawing of the divergent channel is depicted in Fig. 3. The divergence angle is defined as $\beta = \tan^{-1}\frac{H_o - H_i}{L}$. The inlet height and the length of the channel are fixed at $H_i = 12.5\,\text{nm}$ and $L = 250\,\text{nm}$ in lattice units, respectively, with a lattice spacing and time step of $\delta x = \delta t = 0.5$. The channel aspect ratio equals $L/H_i = 20$ which is taken as the same value as the DSMC simulations carried out by Ebrahimi and Roohi.[12] The inlet and outlet pressures are specified using the Zou and He[41] pressure boundary condition. The symmetric boundary condition is applied on the symmetry axis.

Simulation results of the pressure distribution along the channel at an inlet/outlet pressure ratio of $\Pi = 2.5$, and inlet Knudsen number of $Kn_i = 1$ are validated with those of the DSMC in Fig. 4, where an excellent agreement is observed over a wide range of the divergence angle. Furthermore, the pressure distribution is observed to be almost independent of the slip coefficients. As observed, at a fixed pressure ratio,

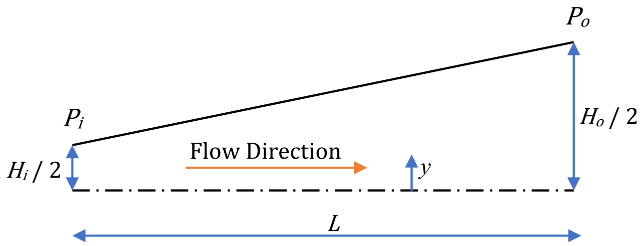

Fig. 3. (Color online) A schematic drawing of the considered problem.

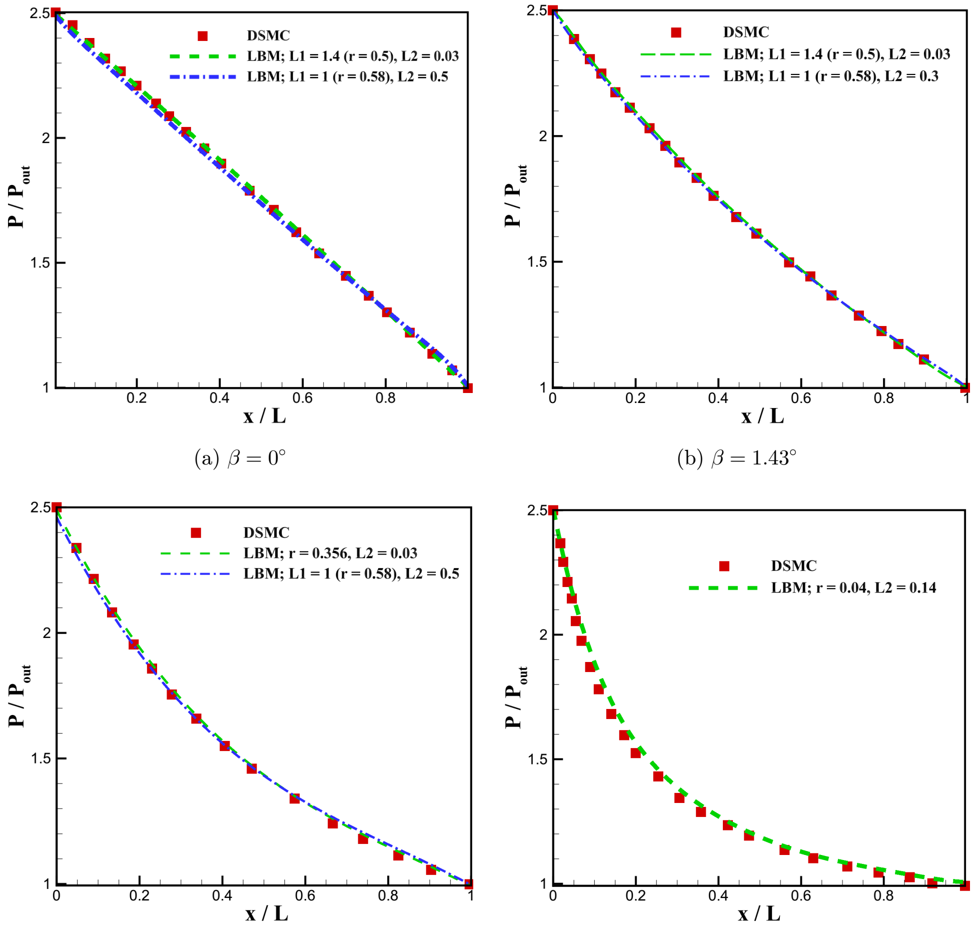

(a) $\beta = 0°$ (b) $\beta = 1.43°$

(c) $\beta = 4.3°$ (d) $\beta = 16.7°$

Fig. 4. (Color online) Comparison of pressure distribution with DSMC results of Ref. 12, $\Pi = 2.5$, $Kn_i = 1$.

the pressure distribution becomes more concave as the divergence angle is increased. This is because the pressure-driven flow is mainly opposed by the viscous forces and the gradual increase of the channel height. Therefore, the pressure falls more rapidly as the angle is increased.

Figure 5 shows the Mach number contour and velocity streamlines at three divergence angles with $\Pi = 2.5$, $Kn_i = 0.3$. As observed, while Knudsen number and as a result Mach number always increase along a straight microchannel in the isothermal pressure driven condition; see Fig. 5(a), an alike trend does not occur necessarily in case of the divergent microchannel where the behavior depends on the pressure ratio and divergence angle. According to values of these two parameters, three scenarios are found to occur in divergent microchannels that are; (1) Mach/Kn

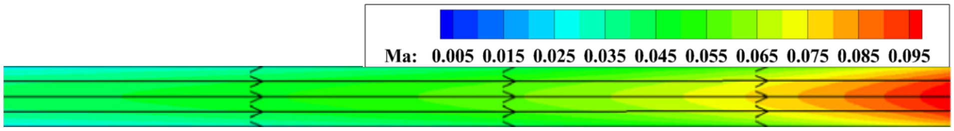

(a) $\beta = 0°$, $r = 0.5$, $L_2 = 0.03$

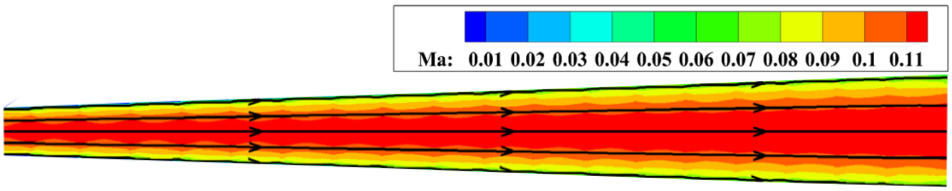

(b) $\beta = 4.3°$, $r = 0.36$, $L_2 = 0.03$

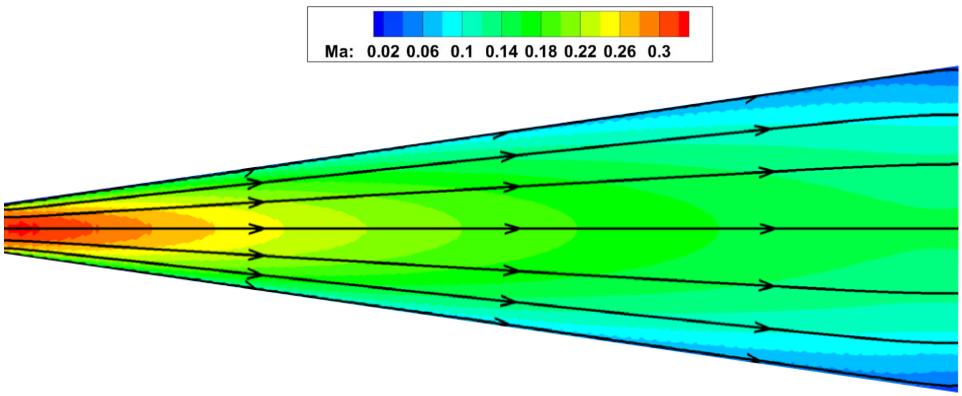

(c) $\beta = 16.7°$, $r = 0.04$, $L_2 = 0.14$

Fig. 5. (Color online) Mach number contours and streamlines at $\Pi = 2.5$ and $Kn_i = 0.3$.

increase similar to straight channels, (2) constant Ma/Kn condition, as shown in Fig. 5(b), and (3) Ma/Kn decrease along the channel, see Fig. 5(c). Therefore, at each pressure ratio, there is a threshold divergence angle where increasing the divergence angles would lead to Ma/Kn reduction and decreasing the divergence angle results in Ma/Kn increases. This angle is discussed and determined in the following section of the paper. Furthermore, no flow separation occurs at $\beta = 16.7°$ due to the slip velocity on the wall.

Variations of the slip and central Mach numbers distribution along the channel for three divergence angles are shown in Figs. 6 and 7, respectively. As observed in Fig. 6, except for $\beta = 16.7$, the LBM results for the slip Mach number are in a good agreement with those of the DSMC only if L_2 is set relatively much smaller than L_1. In other words, the slip velocity should be dominantly adjusted by the value of r, as was expected. Furthermore, the value of r has to be decreased with the increase in the channel angle to produce higher slip velocities predicted by the DSMC results.

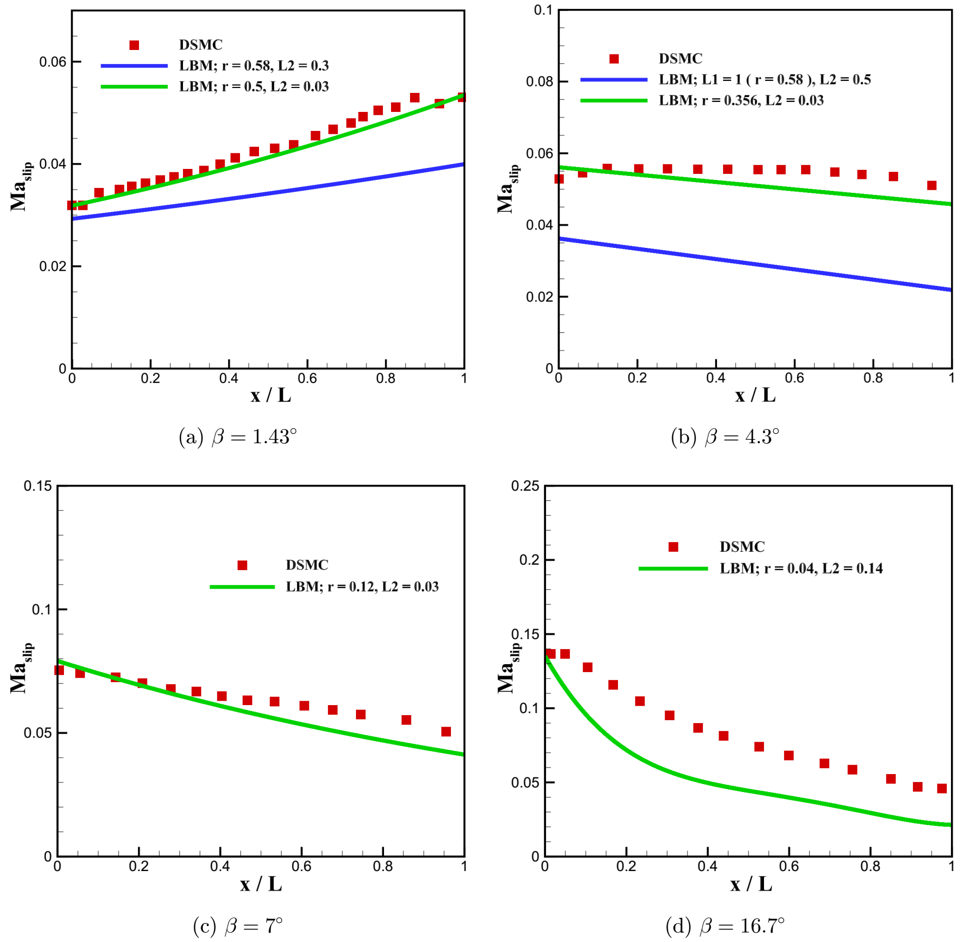

(a) $\beta = 1.43°$ (b) $\beta = 4.3°$

(c) $\beta = 7°$ (d) $\beta = 16.7°$

Fig. 6. (Color online) Slip Mach number variations along the channel at $\Pi = 2.5$, $Kn_i = 1$.

However, results of the slip velocity at $\beta = 16.7$ deviate considerably from the DSMC solutions, even though the value of r is severely reduced. In other words, it was found that at a fixed L_2 magnitude, the slip velocity at this relatively large angle approaches an asymptotic value with decreasing the value of r and the slip is no more increased considerably with further decrease of r. Therefore, it seems that the value of L_2 should be increased to approach the DSMC results, but this will lead to overprediction of the centerline Mach number. Therefore, it can be concluded that the model fails to predict the slip velocity accurately at relatively high divergence angles. However, it will be shown and discussed in what follows that the mass flow rate is predicted very well by the model even at large divergence angles like 16.7 using the same r and L_2 values. From a practical point of view, accurate prediction of the mass flow rate is probably the most crucial feature of a prevailing numerical solver.

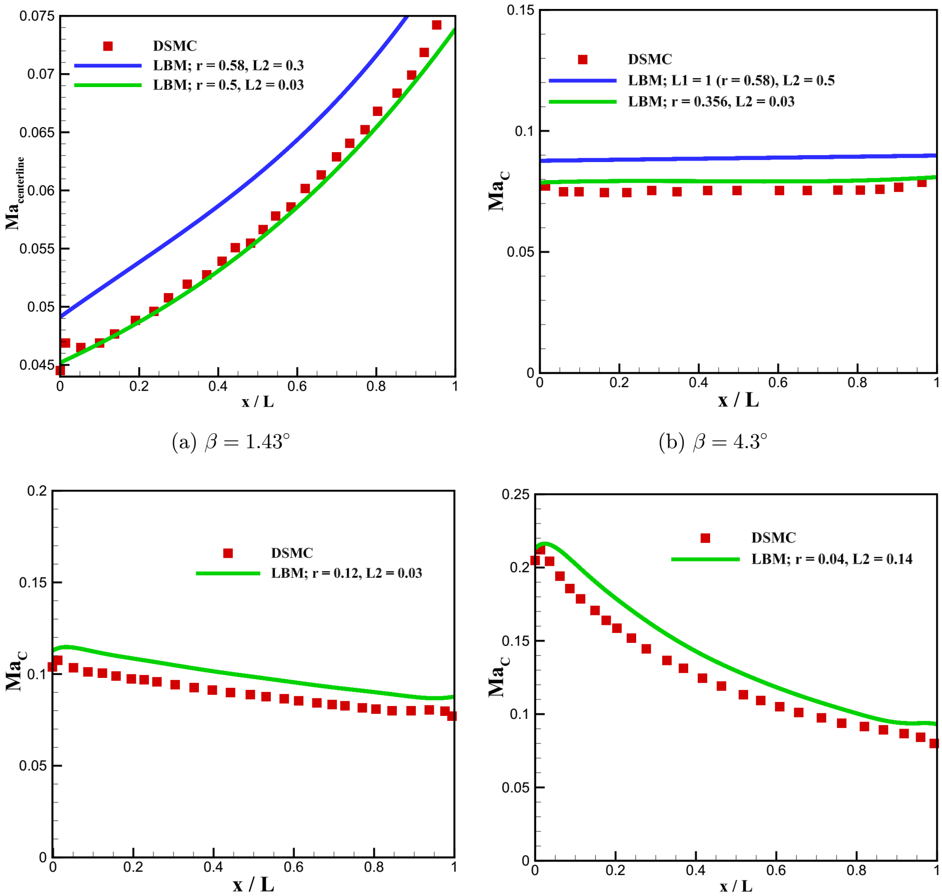

(a) $\beta = 1.43°$ (b) $\beta = 4.3°$

(c) $\beta = 7°$ (d) $\beta = 16.7°$

Fig. 7. (Color online) Centerline Mach number variations along the channel at $\Pi = 2.5$ and $Kn_i = 1$.

Distribution of the Knudsen number along the channel is shown in Fig. 8 for three angles. As observed, variations of the Knudsen number are consistent with those of the slip and centerline Mach numbers at the corresponding angle. It is concluded that the slip and centerline Mach numbers at $\beta = 4.3°$ are nearly constant along the channel due to a constant value of Kn along the channel. According to Eq. (11), Knudsen number remains constant because the pressure drop is compensated by the increase in the channel height. The divergence angle at which the Knudsen number remains constant is found to be dependent only on the pressure ratio.

Figure 9 shows variations of the divergence angle where Knudsen number is constant along the channel, β_c, with the pressure ratio. As observed, the angle increases almost linearly by the pressure ratio. The linear curve fit is

$$\beta_c = 2.82\Pi - 2.7; \;\; 1.5 \leq \Pi \leq 6. \tag{17}$$

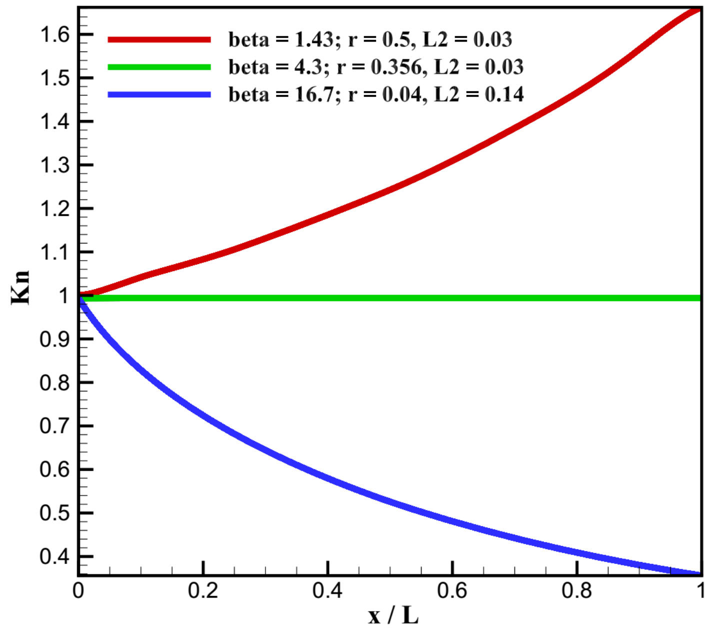

Fig. 8. (Color online) Knudsen number variations along the channel at $\Pi = 2.5$ and $Kn_i = 1$.

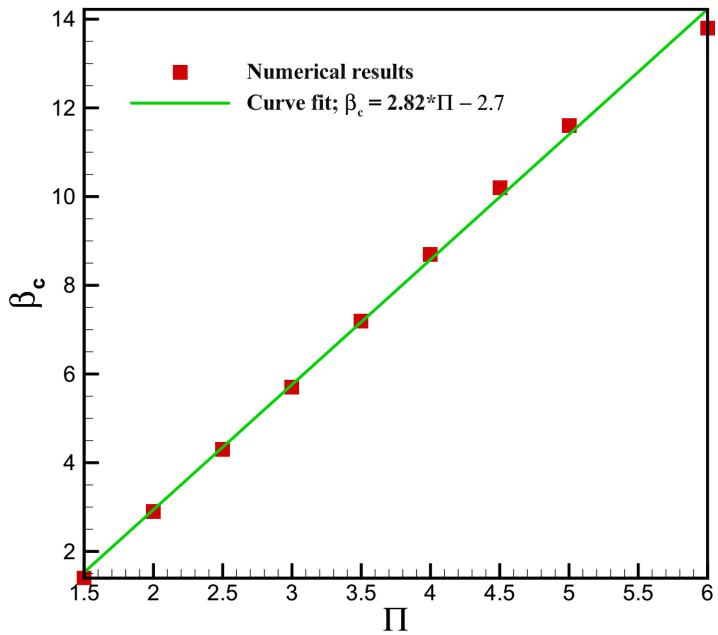

Fig. 9. (Color online) Variations of the divergence angle leading to the constant Kn distribution with the pressure ratio.

Figure 10 shows variations of the non-dimensional mass flow rate, $M_n = \frac{L\sqrt{2RT}}{(P_i - P_o)H_i^2 w}\dot{M}$, with the mean Knudsen number, Kn_m, the latter is calculated at the average pressure of the inlet and outlet. As observed, a very suitable agreement is obtained until $Kn_m \approx 1$ with slip dominated coefficients, but they cannot predict the Knudsen minimum phenomenon. However, the Knudsen minimum is well captured by the model choosing a moderate L_2 value with a good agreement in the entire range of the transition regime. At $\beta = 16.7°$, the Knudsen minimum is weak and the flow rate almost remains constant. Furthermore, as mentioned, even though the model fails to predict the slip velocity properly at this high opening angle, mass flow rate is

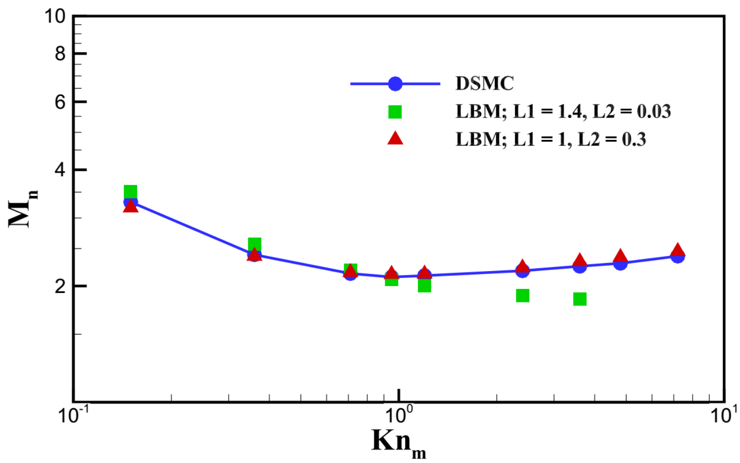

(a) $\beta = 1.43°$

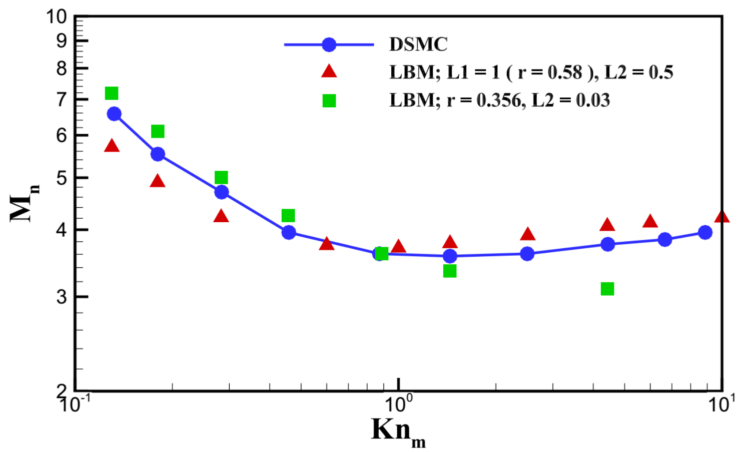

(b) $\beta = 4.3°$

Fig. 10. (Color online) Variations of the nondimensional mass flow rate at $\Pi = 2.5$ and $Kn_i = 1$.

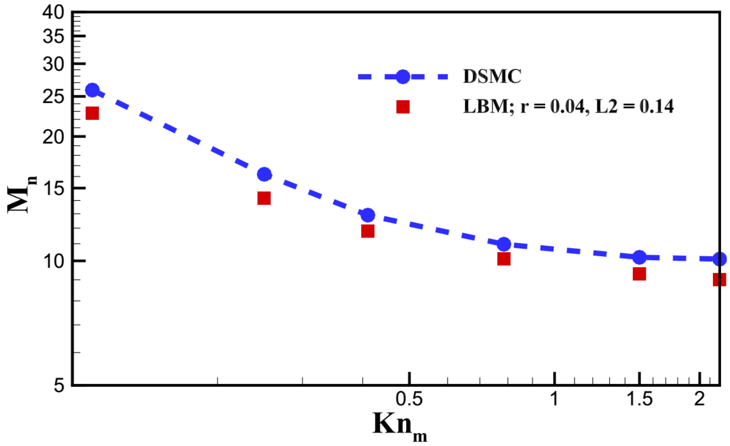

(c) $\beta = 16.7°$

Fig. 10. (*Continued*)

Table 1. Recommended slip coefficients for predicting the mass flow rates at different divergence angles.

$\beta(°)$	r	L_2	Kn_m range	$\text{Error}_{\max}\%$
0	0.58	0.2	Entire transition	6%
1.43	0.58	0.3	Entire transition	3%
4.3	0.356	0.03	0.1–1	10%
4.3	0.58	0.5	Entire transition	13%
7	0.2	0.03	0.1–1	8%
7	0.58	0.5	0.1–5	13%
16.7	0.04	0.14	0.1–2	12%

well estimated by the model. This is because the density (pressure) is considered in the mass flow rate and the overprediction of the centerline Mach number is compensated by the consequent density reduction due to the accurate prediction of the pressure (density) distribution by the model independent of the divergence angle, as depicted in Fig. 4.

Based on the simulation results that are validated with DSMC solutions at $\Pi = 2.5$, the slip coefficients given in Table 1 are suggested to predict the mass flow rates with a suitable accuracy using the current LBM in a wide range of the Knudsen number in the transition regime.

4. Concluding Remarks

The rarefied gaseous flow through diverging micro and nanochannels at different operating conditions and divergence angles was investigated using the TRT LBM. The BSR slip boundary condition was implemented coupled with the second-order slip boundary condition. The divergence wall was approximated with the so-called stair-step Cartesian one and the power law wall function was implemented to capture the Knudsen layer effects. Results were compared with those of DSMC reported in the literature. According to the results, the following conclusions can be made for rarefied flows in diverging micro and nanochannels:

- The local pressure distribution has an excellent agreement with DSMC results in a wide range of the divergence angle almost independent of the slip coefficients.
- There is a specific divergence angle at which the unbounded local Knudsen number and therefore Mach number remain constant along the channel; the angle depends only on the pressure ratio with an almost linear trend.
- The mass flow rate can well be predicted by the current TRT LBM model in a wide range of Kn and divergence angles with an appropriate choice of slip coefficients.
- The Knudsen minimum phenomenon is captured in the divergent channel only by choosing proper slip coefficients.

Acknowledgment

The authors would like to acknowledge the financial support provided by the Faculty of Engineering, Ferdowsi University of Mashhad under Grant No. 47224.

References

1. Y. Zohar, S. Y. K. Lee, W. Y. Lee, L. Jiang and P. Tong, *J. Fluid Mech.* **472**, 125 (2002).
2. C.-I. Weng, W.-L. Li and C.-C. Hwang, *Nanotechnol.* **10**, 373 (1999).
3. N. Dongari, A. Agrawal and A. Agrawal, *Int. J. Heat Mass Transf.* **50**, 3411 (2007).
4. A. Agrawal and A. Agrawal, *Phys. Fluids*, **18**, 103604 (2006).
5. T. Ewart, P. Perrier, I. A. Graur and J. G. MéOlans, *J. Fluid Mech.* **584**, 337 (2007).
6. E. Roohi and M. Darbandi, *Phys. Fluids* **21**, 82001 (2009).
7. N. Singh, N. Dongari and A. Agrawal, *Microfluid. Nanofluid.* **16**, 403 (2014).
8. F. Sharipov and G. Bertoldo, *J. Vac. Sci. Technol. A Vacuum, Surfaces, Film.* **23**, 531 (2005).
9. N. D. Stevanovic, *J. Micromech. Microeng.* **17**, 1695 (2007).
10. V. Hemadri, V. V. Varade, A. Agrawal and U. V. Bhandarkar, *Phys. Fluids* **28**, 22007 (2016).
11. M. Akbari, A. Tamayol and M. Bahrami, *J. Fluids Eng.* **135**, 71205 (2013).
12. A. Ebrahimi and E. Roohi, *Microfluid. Nanofluidics*, **21**, 18 (2017).
13. S. P. Kiselev, V. P. Kiselev and V. N. Zaikovskii, *Shock Waves* **28**, 829 (2018).
14. M. Darbandi and E. Roohi, *Int. Commun. Heat Mass Transf.* **38**, 1443 (2011).
15. A. M. Mahdavi, N. T. P. Le, E. Roohi and C. White, *Numer. Heat Transf. Part A Appl.* **66**, 733 (2014).
16. A. M. Mahdavi and E. Roohi, *Phys. Fluids* **27** 72002 (2015).
17. A. Gavasane, A. Agrawal and U. Bhandarkar, *Vacuum*, **155** 249 (2018).
18. S. Chen and G. D. Doolen, *Annu. Rev. Fluid Mech.* **30**, 329 (1998).
19. X. He and L.-S. Luo, *Phys. Rev. E* **56**, 6811 (1997).
20. P. Lallemand and L.-S. Luo, *Phys. Rev. E* **61**, 6546 (2000).

21. S. Succi, *The Lattice Boltzmann Equation: For Complex States of Flowing Matter* (Oxford University Press, 2018).
22. T. Krüger, H. Kusumaatmaja, A. Kuzmin, O. Shardt, G. Silva and E. M. Viggen, *The Lattice Boltzmann Method* (Springer International Publishing, Cham, 2017).
23. S. F. Kharmiani and M. Passandideh-Fard, *Int. J. Multiph. Flow* **101**, 11 (2018).
24. H. Huang, M. Sukop and X. Lu, *Multiphase Lattice Boltzmann Methods: Theory and Application* (John Wiley & Sons, 2015).
25. S. F. Kharmiani, M. Passandideh-fard and H. Niazmand, *J. Mol. Liq.* **222**, 1172 (2016).
26. J. Harting, C. Kunert and H. J. Herrmann, *Europhys. Lett.* **75**, 328 (2006).
27. A. Montessori, P. Prestininzi, M. La Rocca, G. Falcucci, S. Succi and E. Kaxiras, *J. Comput. Sci.* **17**, 377 (2016).
28. J. Wang, L. Chen, Q. Kang and S. S. Rahman, *Int. J. Heat Mass Transf.* **95**, 94 (2016).
29. A. Agrawal, L. Djenidi and R. A. Antonia, *J. Fluid Mech.* **530**, 135 (2005).
30. T.-M. Liou and C.-T. Lin, *Microfluid. Nanofluid.* **16**, 315 (2014).
31. X. Li, J. Fan, H. Yu, Y. Zhu and H. Wu, *Int. J. Heat Mass Transf.* **122**, 1210 (2018).
32. B. Shi and C. Zheng, *Comput. Math. Appl.* **61**, 3519 (2011).
33. S. Tao and Z. Guo, *Phys. Rev. E* **91**, 43305 (2015).
34. G. Falcucci, S. Succi, A. Montessori, S. Melchionna, P. Prestininzi, C. Barroo, D. C. Bell, M. M. Biener, J. Biener, B. Zugic and E. Kaxiras, *Microfluid. Nanofluid.* **20**, 105 (2016).
35. M. M. Montemore, A. Montessori, S. Succi, C. Barroo, G. Falcucci, D. C. Bell and E. Kaxiras, *J. Chem. Phys.* **146**, 214703 (2017).
36. I. Ginzburg, *Adv. Water Resour.* **28**, 1171 (2005).
37. A. Norouzi and J. A. Esfahani, *Microfluid. Nanofluid.* **18**, 323 (2015).
38. Z. Guo and C. Shu, *Lattice Boltzmann Method and Its Applications in Engineering* (2013).
39. N. Dongari, Y. Zhang and J. M. Reese, *J. Fluids Eng.* **133**, 71101 (2011).
40. B. Shi and C. Zheng, *Comput. Math. Appl.* **61**, 3519 (2011).
41. Q. Zou and X. He, *Phys. Fluids* **9**, 1591 (1997).